

[Click here to view linked References](#)

# Evaluation of black crust formation and soiling process on historical buildings from the Bilbao metropolitan area (North of Spain) using SEM/EDS and Raman microscopy

Estefanía Calparsoro,<sup>1</sup> Maite Maguregui,<sup>2,\*</sup> Anastasia Giakoumaki,<sup>3</sup> Héctor Morillas,<sup>3</sup> Juan Manuel Madariaga<sup>3</sup>

<sup>1</sup> Department of Geography, History and Archaeology, Faculty of Arts, University of the Basque Country UPV/EHU, 01006 Vitoria-Gasteiz, Basque Country, Spain.

<sup>2</sup> Department of Analytical Chemistry, Faculty of Pharmacy, University of the Basque Country UPV/EHU, P.O. Box 450, 01080 Vitoria-Gasteiz, Basque Country, Spain.

<sup>3</sup> Department of Analytical Chemistry, Faculty of Science and Technology, University of the Basque Country UPV/EHU, P.O. Box 644, 48080 Bilbao, Basque Country, Spain.

\*e-mail: [maite.maguregui@ehu.es](mailto:maite.maguregui@ehu.es) phone: +34945013058

## Abstract

In the present work, several building materials suffering from black crusts and soiled surfaces were evaluated by scanning electron microscopy energy dispersive X-Ray spectrometry (SEM-EDS) and micro-Raman spectroscopy. The goal was to examine the elemental and molecular composition, the distribution on the samples and the morphology of endogenous and exogenous compounds on those black crusts and soiled surfaces. The black crusts were deposited over different building materials such as limestone, sandstone and brick that constitute a small construction called “Malacate” as well as over a limestone substrate of a cemetery gate. Both constructions are dated back to the beginning of the twentieth century. The samples of soiling were taken from the façade of a building constructed in the 1980s. The analytical evaluation allowed in a first stage the determination of the composition and the observation of the morphology of soiling and black crusts. In addition, the evaluation of the compositions of the soiling and black crusts of different grade and formation allowed the assessment of the main weathering phenomena that the buildings have suffered, which were found to be: sulfate impact, marine aerosol impact, depositions of metallic particles, crustal particulate matter depositions, carbonaceous particles, biodeterioration and vandalism.

**Keywords:** black crust, soiling, greenhouse acid gases, Raman microscopy, SEM-EDS, Bilbao metropolitan area historical buildings.

## 36 **Introduction**

37 The majority of heritage constructions are constituted by stone and brick materials.  
38 Their outdoor character makes them vulnerable to the atmospheric weathering  
39 phenomena (Doehne and Price 2011) and, among the effects likely to occur, the  
40 formation of black crusts and soiling are of special importance, apart from the  
41 blackening of the surfaces (Brimblecombe and Grossi 2005), because they lead to  
42 physicochemical decay and also act as a pollutant accumulator (Schiavon et al. 2004;  
43 Larseen et al. 2006; Charola et al. 2007; Barca et al. 2010; Barca et al. 2014; Ruffolo et  
44 al. 2015; ) and acting in some cases as natural passive samplers (Morillas et al. 2016a).  
45 Consequently, not only they suppose an aesthetical problem, but in some cases they can  
46 also jeopardize the integrity of a construction. In addition, these crust are prone to  
47 include or accumulate diverse microorganisms and organic compounds in its structure.  
48 Some of these microorganism can bio-synthesize large amounts of hydrated calcium  
49 oxalate (McAlister et al. 2008) or even also promote a physical stress on the building  
50 material (cracks, fissures, etc.) placed at the back of the crust. In fact, it has already  
51 been reported that the accumulation of organic pollutants leads to an increase of  
52 microorganism activity (Potgieter-Vermaak et al. 2005).

53 Black crust growth is due to the formation of gypsum on surfaces sheltered from water  
54 and attacked by SO<sub>2</sub>-polluted atmosphere. According to ICOMOS glossary (ICOMOS  
55 2008), black crust is a “Kind of crust developing generally on areas protected against  
56 direct rainfall or water runoff in urban environment. They are composed mainly of  
57 particles from the atmosphere, trapped into a gypsum matrix (CaSO<sub>4</sub>·2H<sub>2</sub>O)”. On the  
58 other hand, soiling is a “Deposit of a very thin layer of exogenous particles (e.g. soot)  
59 giving a dirty appearance to the stone surface. [...] With increasing adhesion and  
60 cohesion, soiling can transform into a crust” (ICOMOS 2008).

61 The identification of the particulate matter deposited on stone/brick surfaces plays a  
62 crucial role in the understanding of the type of weathering processes suffering or likely  
63 to be suffered by this kind of substrates (Maguregui et al. 2008). At the same time, they  
64 provide significant information about the surrounding atmosphere, reflecting indirectly  
65 the air quality, which has an important effect in the environment as well as in the human  
66 health.

67 The nature of the inorganic salts crystallization occurring in the black crusts and soiling

1  
2  
3  
4  
5  
6  
7  
8  
9  
10  
11  
12  
13  
14  
15  
68 has been widely studied. Works on the field focused on the study of carbon and metallic  
69 particles depositions and on the characterization of the nature of metallic particles  
70 deposited on black crust are increasing in the last years (Sýkorová et al. 2011, Ruffolo  
71 et al. 2015, Morillas et al. 2016a).

72 The present work reports a detailed microscopic and chemical characterization of  
73 different altered stone and brick surfaces to shed light on the deterioration mechanisms  
74 happening on heritage buildings due to the influence of urban polluted and coastal  
75 environments.

76 Regarding the analytical techniques used in the field of building materials analysis, non-  
77 invasive techniques based on micro-spectroscopy have gained ground in the last years.  
78 It is especially important the development carried out in the spectral mapping  
79 techniques for the application on building materials that have suffered impact of  
80 atmospheric pollution such as the following spectroscopic techniques: Raman  
81 spectroscopy, infrared spectroscopy, micro X-Ray fluorescence spectrometry, scanning  
82 electron microscopy coupled to energy-dispersive X-Ray spectrometry (SEM-EDS),  
83 laser ablation inductively coupled plasma mass spectrometry (LA-ICP-MS), etc.  
84 (Watson et al. 2005; Sarmiento et al. 2008; Barca et al., 2010; Barca et al. 2011; Crupi  
85 et al., 2016; Morillas et al. 2016b, Morillas et al. 2016c). Although such techniques are  
86 commonly used in a non-quantitative way, they allow determining the conservation  
87 state of the materials under study in a first stage.

88 For this study, SEM/EDS and micro-Raman spectroscopy were chosen because they  
89 allow obtaining the elemental and molecular composition of the compounds embedded  
90 inside the crust. They also allow visualizing the black crusts appearance as well as the  
91 surfaces that have suffered soiling processes. Furthermore, both techniques allow a  
92 micro-invasive characterization of small samples. Moreover, by Raman spectroscopy it  
93 is possible to discern between different calcium sulfate polymorphs depending on their  
94 hydration states such as gypsum or anhydrite, which are of special relevance concerning  
95 the degradation processes that their dissolution/precipitation cycles may imply  
96 (Rodríguez-Navarro et al. 2000; Flatt et al. 2002; Espinosa-Marzal et al. 2010). The use  
97 of micro-spectroscopic techniques for the study of this type of damaged layers has had  
98 an increase in the last years since it provides reliable information about the composition  
99 of them.

60  
61  
62  
63  
64  
65

100 In the present work, black crusts formed on sandstone, limestone and brick substrates  
101 belonging to one century old constructions were sampled, as well as soiling samples  
102 from an approximately 30 years old building façade. All these historical buildings are  
103 located in the metropolitan area of Bilbao (Basque Country, north of Spain). For the  
104 samples characterization SEM/EDS and micro-Raman spectroscopy techniques were  
105 selected.

106

## 107 **Materials and methods**

### 108 **Sampling**

109 All the studied cases are from buildings located in the municipality of Getxo (Biscay,  
110 North of Spain), which belongs to the metropolitan area of Bilbao (Basque Country,  
111 north of Spain). The sites are in an architecturally noteworthy area situated on the coast,  
112 where the Nerbioi-Ibaizabal estuary finishes. This estuary is the major industrialized  
113 area with the highest population density of the North of Spain. Due to its geographic  
114 situation and because of its mineral resources richness, mainly iron, since the nineteenth  
115 century, this area has suffered the rapid growth of industrialization and population  
116 developments with the subsequent pollution problems. These problems were mainly  
117 manifested since the 1930s, but it was not until after the 1960s, when the inhabitants  
118 started to be aware of them. Despite the improvement of the environmental conditions,  
119 the high rates of air pollution during this period are still obvious in many building  
120 surfaces of the area. In order to study if signs of this pollution are evident on different  
121 kind of crusts formed on buildings, two historical buildings and a more recent one were  
122 selected. In total fifteen samples have been considered for this work. All the samples  
123 have been taken at around 1-1.5 meters from the ground level.

### 124 **Malcate building**

125 This small construction (built around 1900) is one of the remaining constructions that  
126 was built to control the sewage system of Bilbao, as part of the first modern sewage  
127 network of the state. It was a necessary infrastructure for the rapidly growing industrial  
128 society. It was built with rich architectural elements, in terms of materials and structure.  
129 In 1994, the malacate buildings were designated monumental sets of the Basque  
130 Country and in 2004 this specific malacate building located in the municipality of Getxo

131 was included inside the list of historic and architectural heritage properties from the  
132 Basque Country. This building presents black crusts on sheltered areas of the three  
133 materials used for its construction: limestone, sandstone and brick (see Figure 1b). All  
134 these materials covered with black crust were sampled for this work. From each  
135 material showing the presence of black crusts three fragments, a biggest one (around 3 x  
136 3 cm) and two fragments smallest (around 0.5 x 0.5 cm), were taken.

### 137 The Getxo's cemetery gate

138 The Getxo's cemetery gate as the malacate building is already included inside the list  
139 of historic and architectural heritage properties from the Basque Country. This gate of  
140 the beginning of the twentieth century shows black crusts compactly adhered to  
141 sheltered areas of the limestone substrate. It is worth remarking that the gate is situated  
142 opposite to the main rainfall direction (see Figure 1). Three sample fragments of black  
143 crust (one of around 2 x 2 and two of around 0.5 x 0.5 cm respectively) were taken from  
144 these areas.

### 145 Talaieta street building

146 This construction is located in Getxo's downtown (Biscay, North of Spain). It was  
147 constructed during the last decades of the twentieth century and is one of the typical  
148 buildings of the area. It is under the direct influence of road traffic, marine fog and  
149 potential industrial influence. The cantilever does not allow the washing of the zones  
150 that it covers, promoting the concentration of soiling in this part, hence in the present  
151 work was only regarded the lowest part of the building (at around 1 m above ground  
152 level). The damaged façade is constituted by brick shaped limestones. The limestones  
153 with lowest impact show a yellowish color. On the contrary, the most affected ones  
154 show a grayish colour. The natural yellow hue of the stone is given by the presence of  
155 iron as part of its composition. Three fragments of crusts of 3 x 3 (one) and 0.5 x 0.5  
156 (two) cm respectively were taken from the grayish affected area.

### 157 Instrumentation

158 Scanning electron microscopy X-Ray energy dispersive spectrometry  
159 (SEM/EDS) One sample of each different material and location was selected for the  
160 microscopic evaluation. The criteria for the election were both the quantity and the

161 morphology, selecting in this way samples showing the major quantity of crust, and as  
162 much flat as possible. All the considered samples were metallized using gold, and then  
163 studied using an EVO 40 (Carl Zeiss) SEM equipment. The elemental composition of  
164 samples was determined by an energy dispersive EDS, using an X-Max (Oxford  
165 Instruments) equipment. Data were collected at two different voltages of 20 and 30 keV  
166 and a current of 50  $\mu\text{A}$  for the acquisition of images, and 200  $\mu\text{A}$  for the acquisition of  
167 spectra. The working distance ranged between 9 and 11 mm. The EDS spectra were  
168 acquired and treated using the INCA software (Oxford Instruments).

169 The SEM analysis coupled to EDS and processed by the INCA program, permits the  
170 elemental analysis of selected particles previously seen by SEM. Furthermore, a  
171 mapping of specific microscopic areas in the samples is possible, allowing the  
172 evaluation of the distribution of these elements over the sample. Additionally, it  
173 provides semi-quantitative data in terms of weight percentages of the detected elements.  
174 It is necessary to underline that the SEM/EDS semi-quantitative data provided in this  
175 work are just indicative and cannot be considered completely quantitative because no  
176 reference materials/standards were used to perform an empirical calibration.

### 177 Micro Raman spectroscopy

178  
179 For the micro-Raman measurement of biggest crust samples, a Raman Renishaw RA  
180 100 spectrometer, with an excitation wavelength of 785 nm (diode laser) and a Peltier  
181 cooled CCD detector was used for the molecular characterization of the samples. The  
182 system was calibrated daily using the 520  $\text{cm}^{-1}$  silicon line. In order to avoid thermal  
183 decomposition of samples, the laser power (150 mW maximum) was kept in low levels,  
184 mainly between 1.5 to 15 mW, depending on the sample.

185 The spectral resolution was 4  $\text{cm}^{-1}$  in the range between 3000–200  $\text{cm}^{-1}$  and the spectra  
186 were acquired randomly on the crusts under study by accumulating from 5 to 20 scans  
187 to improve the signal-to-noise ratio. Due to a microscope lens built in the microprobe  
188 (objective lenses of: 4 $\times$ , 20 $\times$ , 50 $\times$ ) and a video-camera, a proper focusing of the laser  
189 beam spot is possible (approximately 10–200  $\mu\text{m}$ , depending on the focusing lens). Data  
190 acquisition was carried out with the Wire 3.0 software package (Renishaw, UK) and the  
191 analysis of the results was performed using the Omnic V.7.2. software (Nicolet).

192 Additionally, a portable Raman spectrometer (innoRam B&WTEK<sub>INC.</sub>) was used for the  
193 measurement of the smallest crust samples. This spectrometer implements a 785 nm  
194 excitation laser source and has a variable power range up to 300 mW. The probe offers  
195 also the possibility to perform microscopic analysis mounting it on a micro-camera and  
196 using different objective lenses (20× and 50×) that allow measuring areas of a diameter  
197 between 10 and 200 μm. In contrast to the RA 100 spectrometer, with this instrument  
198 samples can be placed under the objective lens to acquire the Raman spectra. With the  
199 RA100 spectrometer, samples must be placed vertically on a support to perform the  
200 spectral acquisition. This sample positioning could be more difficult for small samples  
201 (0.5 x 0.5 cm), thus it was decided to measure them using the portable innoRam  
202 spectrometer available in the laboratory.

203 Finally, in the cases where the 785 nm excitation wavelength was giving a weak Raman  
204 signal, a 514 nm excitation wavelength (50 mW nominal laser power) was used. With  
205 this purpose, an inVia Renishaw confocal Raman micro-spectrometer (Renishaw,  
206 Gloucestershire, UK) coupled to a DMLM Leica microscope with a variety of objective  
207 lenses (20×, 50×, and 100×) to choose and a Peltier cooled CCD detector which  
208 implements a 514 nm excitation wavelength laser was used.

209 The interpretation of the acquired Raman spectra was carried out by comparison with  
210 the Raman spectra of standard samples that are registered in the dispersive Raman  
211 spectroscopic database of e-VISNICH (Maguregui et al. 2010a) and comparing with  
212 free Raman databases (e.g. RRUFF (Downs and Hall-Wallace 2002)).

## 213 214 **Results and discussion** 215

216 In the Table 1, a summary of the main results obtained for the crusts samples of the  
217 three building located in the municipality of Getxo, in the Bilbao metropolitan area,  
218 after the application of the proposed analytical methodology is presented.

219  
220  
221

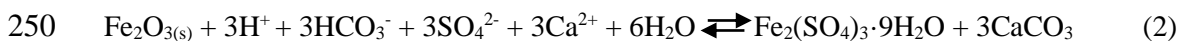
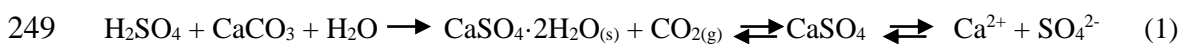
222 Black crust of Malacate building

223 Raman characterization

224 Gypsum (CaSO<sub>4</sub>-H<sub>2</sub>O) was the main constituent identified on the black crusts growing  
225 on the three building materials from the malacate building, which can be formed as a  
226 consequence of the transformation of calcite (CaCO<sub>3</sub>) in the presence of atmospheric  
227 sulfur oxide (wet or dry deposition) (Morillas et al. 2016d; Morillas et al. 2016e).  
228 Moreover, several iron oxides were characterized. Hematite (Fe<sub>2</sub>O<sub>3</sub>) was found on all  
229 three substrates, with major presence in the case of limestone, pointing out the exposure  
230 of the building to Fe rich particles. Moreover, magnetite (Fe<sub>3</sub>O<sub>4</sub>) was also detected on  
231 samples of the black crust on limestone. The size of the magnetite particles identified  
232 ranges from 5-50 μm. Thus, it can be considered that isolated spherules and  
233 agglomerates could be present on the black crusts formed on the limestone. Magnetite  
234 can be associated with atmospheric particles in the urban environment. They are mainly  
235 derived from combustion processes such as industrial, domestic and vehicle emissions  
236 or from abrasion products from asphalt and from vehicle brake systems (Gautam et al.  
237 2005).

238 Additionally, Raman spectroscopic analysis performed in black crusts on the brick,  
239 revealed the presence of a band at 1025 cm<sup>-1</sup>. Using Raman spectroscopy it has been  
240 proven that iron (III) oxide is present in the original brick composition (see Raman  
241 bands related with hematite in Figure 2A). The band at 1025 cm<sup>-1</sup> can be related with  
242 (para)coquimbite (Fe<sub>2</sub>(SO<sub>4</sub>)<sub>3</sub>·9H<sub>2</sub>O), which is a degradation compound formed due to  
243 the attack of sulfuric acid aerosol (sulfur dioxide wet deposition) to iron oxides  
244 (Maguregui et al. 2011). The atmospheric sulphur oxides (SO<sub>x</sub>), usually reacts firstly  
245 with the ions of calcium providing gypsum and, later this gypsum starts reacting with  
246 the iron oxides providing (para)coquimbite, following the reactions (1) and (2)  
247 (Maguregui et al. 2010b).

248



251



1  
2  
3  
4  
5  
6  
7  
8  
9  
10  
11  
12  
13  
14  
15  
16  
17  
18  
19  
20  
21  
22  
23  
24  
25  
26  
27  
28  
29  
30  
31  
32  
33  
34  
35  
36  
37  
38  
39  
40  
41  
42  
43  
44  
45  
46  
47  
48  
49  
50  
51  
52  
53  
54  
55  
56  
57  
58  
59  
60  
61  
62  
63  
64  
65

252 According to this reaction, it is supposed to be normal to find (para)coquimbite together  
253 with gypsum and hematite, as they are the reactants of this degradation product (see the  
254 spectra in the Figure 2A).

255 It is very difficult to distinguish among Raman spectra of coquimbite and  
256 paracoquimbite, because they are quite similar. Both are iron (III) sulfate non-hydrates  
257 and they are also polytypes (a special kind of polymorphism, in which the two  
258 polymorphs differ only in the stacking of identical two-dimensional sheets or layers).

259 The Raman band at  $1025\text{ cm}^{-1}$  can be also related with  $\gamma$ -anhydrite ( $\gamma\text{-CaSO}_4$ ) (Wein et  
260 al. 2014). In the same spectrum where this band was identified, the main band of  
261 gypsum is also present (see Figure 2A). This observation could also suggest that  
262 gypsum is suffering a dehydration process, giving rise to the anhydrous form. Anhydrite  
263 is usually crystallized as  $\beta$ -anhydrite. According to some authors, the environmental  
264 temperature and the internal stress of the material could have influence in the  
265 dehydration process of gypsum, causing the crystallization of the  $\beta$  or  $\gamma$ -anhydrite phase  
266 (Comodi et al. 2012; Prieto-Taboada et al. 2014).

267 The calcite ( $\text{CaCO}_3$ ) identified in the brick can arise from the carbonation process of the  
268 hydrated calcium oxide ( $\text{Ca(OH)}_2$ ), present in the brick, which can be subsequently  
269 sulfated (Maguregui et al. 2009). Calcite can also be present as a consequence of its  
270 deposition on the brick as airborne particulate matter. Unfortunately, it has not been  
271 possible to identify calcite on the surface of the brick. Another calcium source could be  
272 the remnant calcium carbonate, which has not been completely decomposed into  
273 calcium oxide ( $\text{CaO}$ ) during the firing process of the clay from the brick.

274 Furthermore, several spectra of amorphous carbon were acquired both from the  
275 limestone's and sandstone's black crusts. The literature reports that in the carbonaceous  
276 content appearing in the black crusts, the organic carbon fraction is usually higher than  
277 the elemental fraction in most cases due to a great number of microscopically detectable  
278 microorganisms and carbonaceous particles from the atmosphere including organic  
279 compounds bound in the surface layer (aliphatic hydrocarbons, polycyclic aromatic  
280 hydrocarbons, terpenoid derivatives, etc.) (Saiz-Jimenez et al 1991; Bonazza et al.  
281 2007).

1  
2  
3  
4  
5  
6  
7  
8  
9  
10  
11  
12  
13  
14  
15  
16  
17  
18  
19  
20  
21  
22  
23  
24  
25  
26  
27  
28  
29  
30  
31  
32  
33  
34  
35  
36  
37  
38  
39  
40  
41  
42  
43  
44  
45  
46  
47  
48  
49  
50  
51  
52  
53  
54  
55  
56  
57  
58  
59  
60  
61  
62  
63  
64  
65

282 Additionally, the presence of other compounds, coming from anthropogenic sources,  
283 was also identified in the black crusts from limestone. These are phtalocyanine blues, a  
284 phtalocyanine (C<sub>32</sub>H<sub>18</sub>N<sub>8</sub>) based compound, widely used in the dying industry. Black  
285 diamond pigment, based on carbon black pigment was also detected. Both are  
286 commercial pigments and were ascribed to graffitii residues. Through Raman  
287 spectroscopy, burnt sienna was also identified. This is an earth pigment that takes its  
288 name from the heated version of raw sienna which contains iron oxide and manganese  
289 oxide (Genestar and Pons, 2005). Nevertheless, the origin of burnt sienna is not  
290 completely clear, since this could be a constituent of the limestone as well, since they  
291 are similar from the mineralogical viewpoint.

## 292 SEM/EDS evaluation

293 In the black crust samples from Malacate building sandstone, a smooth and compact  
294 carbon layer with some pores from where the underlying gypsum crystals are  
295 observable can be appreciated (see Figure 3A and 3B). Furthermore, depositions of Al-  
296 silicates, quartz ( $\alpha$ -SiO<sub>2</sub>), calcite and those ascribed to sea aerosol containing Na, Mg,  
297 K and Cl were characterized on the surface. Concretely, in the Figure 3C a Cl particle  
298 inserted in the pores of the carbon layer of the black crust can be observed (see Figure  
299 3C and 3D). These finding evidences that the particles coming from the marine aerosol  
300 can be deposited and trapped in the black crust matrix (Morillas et al. 2016a).

301 With regard to the limestone's black crust, carbon was not present as a smooth and  
302 compact layer (see EDS carbon map in Figure S1 from Supplementary Material) like in  
303 the black crust from sandstone. In this case, the contribution of calcite depositions  
304 ascribed to the crustal particulate matter was observed over calcite crystals, which  
305 seemed to have been recrystallized during the black crust formation. In Figure 4,  
306 examples of particles deposited on the black crust can be observed. According to the  
307 semi-quantitative information included in Table 2 and EDS spectral evidences presented  
308 in Figure 4, not only individual particles of gypsum (see EDS Figure 4B and Table 2),  
309 and calcite (see Figure 4C and Table 2) were identified on the limestone's black crust,  
310 but also aggregate particles including aluminosilicates, sulfates and chlorine (see Figure  
311 4A and Table 2)

312

313

314 Black crusts of the cemetery gate

315

316 Raman characterization

317

318 Raman spectroscopy allowed the identification of gypsum, hematite and magnetite as  
319 the main components of the black crusts from the cemetery gate. Gypsum crystals and  
320 hematite particles are distributed to a great extent in the black crust, indicating that this  
321 building has been influenced by a highly polluted environment. Additionally,  
322 carotenoids were also identified embedded in the black crusts, indicating that  
323 microorganisms are included inside the matrix of the black crust. These colonizers are  
324 able to excrete organic pigments, called carotenoids, or they can be present in its  
325 biological structure. Only having the two main Raman bands of carotenoids it is quite  
326 difficult to ascribe this Raman signal to a specific carotenoid, but as it is shown in  
327 Figure S2 from Supplementary Material, this signal could belong to  $\beta$ -carotene.

328

329 SEM/EDS evaluation

330

331 The black crust in the cemetery gate was constituted by a matrix of gypsum crystals  
332 with depositions of carbon and random particles (see Figure 5B, where the carbon layer  
333 is highlighted in red). According to the literature, this is the most characteristic case of  
334 black crust (Moropoulou et al. 1998). The average size of the acicular gypsum crystals  
335 of the matrix (see Figure 5A) is circa 30  $\mu\text{m}$  long and 5  $\mu\text{m}$  wide.

336 Apart from the ubiquitous gypsum, EDS analysis performed on different particles  
337 deposited on the gypsum matrix showed that most of the particles consist mainly of  
338 aluminosilicates of Ca and K (see Figure 5C). These compounds can come from the  
339 physical and chemical weathering of soils and rocks, then being transported by the wind  
340 and finally been deposited in the façades. In atmospheric geochemistry this kind of  
341 compounds is known as crustal particulate matter (Querol et al. 2011) and comprises the  
342 44% of global emissions of particulate matter (PM) to the atmosphere (Inza-Agirre  
343 2010). Some of the particles (see particle 2 in Figure 5C) show the presence of S and Cl  
344 apart from aluminosilicates and most of them also contain traces of metals such as Fe,  
345 Zn, Ti and Mn (see Figure 5C). Elements like S (from sulfates) and Cl (from chlorides)  
346 can come from particles emitted by marine aerosol (Morillas et al. 2016e). The first  
347 element linked with sulfates can come also from anthropogenic emissions or also from

1  
2  
3  
4  
5  
6  
7  
8  
9  
10  
11  
12  
13  
14  
15  
16  
17  
18  
19  
20  
21  
22  
23  
24  
25  
26  
27  
28  
29  
30  
31  
32  
33  
34  
35  
36  
37  
38  
39  
40  
41  
42  
43  
44  
45  
46  
47  
48  
49  
50  
51  
52  
53  
54  
55  
56  
57  
58  
59  
60  
61  
62  
63  
64  
65

348 calcium carbonate crustal particles that can be transformed in the atmosphere into  
349 sulfates by reaction with the H<sub>2</sub>SO<sub>4</sub> (coming from SO<sub>x</sub> emission) present in the acid  
350 rain (Morillas et al. 2016e).

351 The length of the particles varies in the range of 5 to 15 μm approximately. Apart from  
352 the hazards that the pollutants can cause to the human health due to their toxicity (e.g.  
353 heavy metals) their size can be also crucial as far as the hazardousness is concerned; the  
354 smaller the particles are, the worse is the effect caused on human health. The PM<sub>10</sub>  
355 particles (those sizing less than 10 μm) are more hazardous than the bigger ones, since  
356 they are difficult to expel (especially from the human body). Moreover, the particles  
357 below 2.5 μm (PM<sub>2.5</sub>) are even more hazardous, since, once inhaled, they reach directly  
358 the blood system (Inza-Agirre 2010; EPA 2016).

359 The composition of particle 4 in Figure 5A is given in the pie chart (Figure 5D). It gives  
360 an idea of the nature of this kind of aggregates deposited on the surface. Apart from the  
361 elements mentioned before, here we can see the contribution of Na, Cl and Mg, ascribed  
362 to the chlorides coming from marine fog.

363 This is an example of how airborne particulate matter in form of deposition is mixed  
364 with particles from both anthropogenic and natural sources. It cannot be predicted if the  
365 aggregate has been formed in the atmosphere, or once deposited on the gypsum matrix.  
366 Nevertheless, the airborne particulate matter tends to sediment once it has reached the  
367 aerodynamic diameter of 20 μm. Indeed, the particles with higher diameter are called  
368 sedimentable particles and they are characterized by their short time in the atmosphere,  
369 which is of about some hours (Inza-Agirre 2010). Therefore, either the source is in the  
370 proximity of the building or it has been formed once deposited, acting as a nucleation  
371 point.

372  
373 **Soiling process of the Talaieta street building**

374  
375 **Raman characterization**

376  
377 A big variety of compounds were identified in this building's samples through Raman  
378 microscopy. The presence of iron oxides such as hematite (see Figure 2C) and  
379 magnetite, detected in abundance, was ascribed to the deposition of particulate matter.  
380 Silicates, among them quartz and feldspars, such as adularia and sanidine alkali

1  
2  
3  
4  
5  
6  
7  
8  
9  
10  
11  
12  
13  
14  
15  
16  
17  
18  
19  
20  
21  
22  
23  
24  
25  
26  
27  
28  
29  
30  
31  
32  
33  
34  
35  
36  
37  
38  
39  
40  
41  
42  
43  
44  
45  
46  
47  
48  
49  
50  
51  
52  
53  
54  
55  
56  
57  
58  
59  
60  
61  
62  
63  
64  
65

381 feldspars ( $\text{KAlSi}_3\text{O}_8$ ), were also identified as particulate matter deposition and more  
382 specifically as crustal particular matter. The bands between 1200 and 1600  $\text{cm}^{-1}$  in  
383 Figure 2D were initially ascribed to silicates in general, but there is an open discussion  
384 about the topic, and the latest assumptions are that they might be fluorescence signals  
385 arising from impurities that are actually in silicate matrices, but not directly resulting  
386 from silicates (Gómez-Nubla et al. 2013). In fact, in a measurement acquired with a 532  
387 nm laser, they should not appear for this same reason.

388 Degradation products deriving from the interaction between atmospheric pollutants and  
389 the calcareous stone surface were also identified, such as gypsum and anhydrite (see  
390 Figure 2D). The presence of calcium sulfates with different hydration states could  
391 suggest that the hydration/dehydration cycle of gypsum-anhydrite is taking place (in this  
392 case bassanite was not identified). This cycle produces tension in the material due to a  
393 volume change on the stone and can promote cracks, fissures and fractures on the  
394 material.

395 Apart from the exogenous compounds ascribed to degradation processes and  
396 atmospheric depositions, some remains of graffiti painting were found. For instance, the  
397 presence of ultramarine blue pigment was confirmed by Raman spectroscopy (see  
398 Figure 2A).

### 399 SEM/EDS evaluation

400 At a first stage, the brownish crust present in the Talaieta street building is formed by  
401 several randomly arranged particles which do not show strong cohesion as in the rest of  
402 the buildings. In this case, there is not an evident gypsum crystals layer. In Figure 6A  
403 and 6B, Ca, Si and S EDS maps can be observed. As can be appreciated in the overlaid  
404 EDS map, Ca is spread over the sample whereas there is predominance in S over Si  
405 matching with Ca map. Considering this, it is assumed that the crust is a mixture of  
406 gypsum and silicates.

407 Different subtractions were made on the same EDS maps (in Figure 5A and 5B)  
408 revealing spots with high amount of Ca, which did not match neither with S nor with Si.  
409 Therefore, they were ascribed to possible calcite depositions. Furthermore, several Si  
410 accumulation points were also spotted depicting possible quartz depositions. The  
411 assumption of being deposited rather than belonging to the substrate is made taking into

1  
2  
3  
4  
5  
6  
7  
8  
9  
10  
11  
12  
13  
14  
15  
16  
17  
18  
19  
20  
21  
22  
23  
24  
25  
26  
27  
28  
29  
30  
31  
32  
33  
34  
35  
36  
37  
38  
39  
40  
41  
42  
43  
44  
45  
46  
47  
48  
49  
50  
51  
52  
53  
54  
55  
56  
57  
58  
59  
60  
61  
62  
63  
64  
65

412 account the minimum penetration depth of the X-Ray beam of the EDS.

413 EDS spectra indicate a high input of metallic airborne particulate matter. Al, Ca, Fe, K,  
414 Ti, Zn, Cu, Pb, Cr, Mn and V were identified. Among them, titanium particles were the  
415 most abundant, regularly accompanied by Fe and traces of Pb and V (see Figure 6F).

416 Apart from the Al-silicates encountered repeatedly among the EDS analysis, EDS  
417 spectra, acquired on the particle circled in Figure 6D of more heterogeneous nature and  
418 with a diameter of about 3  $\mu\text{m}$ , showed gypsum as one of the main constituents of the  
419 particle, but also the presence of fluorine (around 22% in weight). The origin of the  
420 fluorine is not clear. Fluorides are naturally occurring components (in rocks, soils, etc.)  
421 and they can enter the atmosphere through volcanic emissions and the re-suspension of  
422 soil by the wind. Marine aerosols also release small amounts of gaseous hydrogen  
423 fluoride and fluoride salts into the air (Franzén 1990; Stefanis et al. 2005). Moreover, it  
424 may come from anthropogenic sources such as industry, incinerators, etc. Indeed,  
425 fluorine identified on the surface of a building located in Getxo, may come from a  
426 factory (where fluorine compounds are produced), as has been reported (Martínez-  
427 Arkarazo et al. 2007).

428 With regard to the metallic elements distribution, the predominant element was found to  
429 be iron as is depicted in Figure 6C (Fe particles are highlighted in blue). This spot was  
430 considered as representative of the sample as this behavior is extended along the  
431 surface. These maps contribute to know the way in which metallic particles are  
432 deposited. At this spot, Mn, Fe and Ti-rich particles are shown. Iron is clearly the most  
433 abundant element, being deposited in a wide range of different particle sizes, which  
434 range from 1  $\mu\text{m}$  long to a diameter of 20-25  $\mu\text{m}$  approximately. The EDS spectrum of  
435 the Fe particle particularly, revealed the contribution of other metals such as Zn and  
436 traces of Pb (see Figure 6F).

437 In addition to Fe, titanium particles with acicular shape of 20  $\mu\text{m}$  long approximately  
438 can be observed (see Figure 6C). And finally, manganese is present in a minor extent  
439 with an average size of around 5  $\mu\text{m}$ . The EDS spectrum of the Mn particle revealed  
440 that it is composed mainly of Mn, without any contribution of other metals, in  
441 contradiction to the cases of other aggregates.

442 Thanks to the EDS maps, through correlation of the elements, it was possible to

1  
2  
3  
4  
5  
6  
7  
8  
9  
10  
11  
12  
13  
14  
15  
16  
17  
18  
19  
20  
21  
22  
23  
24  
25  
26  
27  
28  
29  
30  
31  
32  
33  
34  
35  
36  
37  
38  
39  
40  
41  
42  
43  
44  
45  
46  
47  
48  
49  
50  
51  
52  
53  
54  
55  
56  
57  
58  
59  
60  
61  
62  
63  
64  
65

443 evaluate the different kinds of depositions apart from those mentioned before. On the  
444 one hand, the influence of marine aerosol is obvious. The EDS maps of Na, Cl and also  
445 Mg are quite coincident, suggesting deposition of halite (NaCl) and MgCl (see Figure  
446 S3 from Supplementary Material). Moreover, in some microscopic areas from the Na  
447 and Cl EDS maps, both elements distribution is coincident pointing out the presence of  
448 halite (NaCl) crystal (see Figure S3 from Supplementary Material). On the other hand,  
449 the depositions of aluminosilicates are shown in the EDS maps of Al and Si (see Figure  
450 S3 from Supplementary Material). Furthermore, the distribution of Fe and Ti, highlight  
451 again the high rate of metallic depositions on the sample (see Figure S3 from  
452 Supplementary Material). Finally, the C map showed an accumulation, which indicates  
453 the presence of carbonaceous particles, probably corresponding to soot (see Figure S3  
454 from Supplementary Material).

455 In order to perform a comparative analysis of the elemental composition from each  
456 representative crust extracted from the three buildings, three selected areas from each  
457 crust sample (one from each building) were analyzed by EDS. For each crust sample,  
458 the semi-quantitative information from the three selected areas was obtained and an  
459 average value was calculated for each building crust sample. In Figure 7 a  
460 representative SEM image of each building crust sample is shown together with the  
461 semi-quantitative values (average) obtained from each building crust sample. The  
462 results pointed out that the major concentration of sulfur was present in the cemetery  
463 gate's black crust. Hence, it is assumed that the limestone of the cemetery has been  
464 exposed to an atmosphere rich in SO<sub>x</sub> acid aerosols for a longer period of time  
465 comparing with the rest of the building, with the proper conditions to commence an  
466 important sulfation process, enhancing in this way the formation of crystals that are,  
467 doubtless, the best formed crystals comparing to the rest of the samples in terms of size  
468 and crystal structure (see SEM image 3 In Figure 7 showing the sulfate crystals from the  
469 cemetery gate's black crust in comparison with the crusts of the other two buildings).

470  
471  
472

## Conclusions

473 Through the evaluation of the different patterns of weathering processes –all due to  
474 atmospheric influence– among the analyzed façades, it was determined that the  
475 presence of sulfates was massive in the case of limestone's black crusts and minor in the

1  
2  
3  
4  
5  
6  
7  
8  
9  
10  
11  
12  
13  
14  
15  
16  
17  
18  
19  
20  
21  
22  
23  
24  
25  
26  
27  
28  
29  
30  
31  
32  
33  
34  
35  
36  
37  
38  
39  
40  
41  
42  
43  
44  
45  
46  
47  
48  
49  
50  
51  
52  
53  
54  
55  
56  
57  
58  
59  
60  
61  
62  
63  
64  
65

476 case of other materials. Despite the minor presence of sulfates,, the hazardousness of the  
477 identified anhydrite plays a crucial role in the soiling of Talaieta street building due to  
478 the dissolution/precipitation processes that can suffer this kind of sulfate.

479 All the cases showed the influence of marine aerosols, being the case of Talaieta street  
480 building the most affected one. In this case, the contribution of marine aerosols may  
481 have played a negative role in the formation of the crust (contribution of airborne  
482 particulate matter).

483 Carbonaceous particles associated to the nearby preexisted railway and road traffic were  
484 found in a great extent in the crusts formed on the sandstone from the Malacate  
485 building. These particles have formed a smooth compact layer over the gypsum crystals  
486 of the crust.

487 Regarding the rate of depositions, the most recently constructed building is the most  
488 affected by the depositions of airborne particulate matter, depicting the highest  
489 susceptibility (among the studied substrates) that have been ascribed to the low quality  
490 of the building material associated to the high percentage of aluminosilicates in the  
491 substrate.

492 The Malacate construction has been exposed to a polluted atmosphere rich in SO<sub>x</sub> and  
493 iron particles, as the advanced stages of the crusts indicates the presence of hematite,  
494 magnetite and (para)coquimbite.

495 The cemetery gate has undergone the formation of a crust, which also hosts  
496 microorganisms/colonizers, depicting a complex black crust matrix.

497 The use of molecular and elemental spectroscopic techniques allowed the determination  
498 of the degradation state of the substrates due to the formation of soiling and black  
499 crusts. Moreover, micro-Raman spectroscopy together with SEM/EDS has proven to be  
500 a reliable combination for the assessment of the depositions of airborne particulate  
501 matter and the degradation products formed due to the impact of atmospheric pollutants,  
502 as well as any other inputs such as graffiti for example.

503 The use of micro-Raman spectroscopy results in a valuable resource for this kind of  
504 crusts, especially regarding the characterization of crustal particulate matter such as  
505 hematite and magnetite, feldspars such adularia, sanidine and other kind of Al-silicates



1  
2  
3  
4  
5  
6  
7  
8  
9  
10  
11  
12  
13  
14  
15  
16  
17  
18  
19  
20  
21  
22  
23  
24  
25  
26  
27  
28  
29  
30  
31  
32  
33  
34  
35  
36  
37  
38  
39  
40  
41  
42  
43  
44  
45  
46  
47  
48  
49  
50  
51  
52  
53  
54  
55  
56  
57  
58  
59  
60  
61  
62  
63  
64  
65

506 as well as calcium sulfates.

507

## 508 **Acknowledgements**

509 This work has been funded by the Spanish Ministry of Economy and Competitiveness  
510 (MINECO) through the project DISILICA-1930 (ref.BIA2014-59124-P) and the  
511 Regional Development Fund (FEDER). E. Calparsoro is grateful also to Spanish  
512 Ministry of Economy and Competitiveness (MINECO) who funded his pre-doctoral  
513 fellowship (ref: BES-2014-068940). Technical support provided by the Raman-  
514 LASPEA laboratory of the SGIker (UPV/EHU, MICINN, GV/EJ, ERDF and ESF) is  
515 also gratefully acknowledged.

516

## 517 **References**

- 518 Barca D, Belfiore CM, Crisci GM, La Russa MF, Pezzino A, Ruffolo SA (2010)  
519 Application of laser ablation ICP-MS and traditional techniques to the study of black  
520 crusts on building stones: a new methodological approach. *Environ Sci Poll Research*  
521 17:1433–1447
- 522 Barca D, Belfiore CM, Crisci GM, La Russa MF, Pezzino A, Ruffolo SA (2011) A new  
523 methodological approach for the chemical characterization of black crusts on building  
524 stones: a case study from the Catania city centre (Sicily, Italy). *J Anal At Spectrom*  
525 26:1000–1011
- 526 Barca D, Comite V, Belfiore C.M, Bonazza A, La Russa M.F, Ruffolo S.A, Crisci G.M,  
527 Pezzino A, Sabbioni C (2014) Impact of air pollution in deterioration of carbonate  
528 building materials in Italian urban environments. *App Geochem* 48:122-131
- 529 Bonazza A, Brimblecombe P, Grossi CM, Sabbioni C (2007) Carbon in Black Crusts  
530 from the Tower of London. *Environ Sci Technol* 41:4199–4204
- 531 Brimblecombe P, Grossi CM (2005) Aesthetic thresholds and blackening of stone  
532 buildings. *Sci Total Environ* 349:175-189

- 1  
2  
3  
4  
5  
6  
7  
8  
9  
10  
11  
12  
13  
14  
15  
16  
17  
18  
19  
20  
21  
22  
23  
24  
25  
26  
27  
28  
29  
30  
31  
32  
33  
34  
35  
36  
37  
38  
39  
40  
41  
42  
43  
44  
45  
46  
47  
48  
49  
50  
51  
52  
53  
54  
55  
56  
57  
58  
59  
60  
61  
62  
63  
64  
65
- 533 Charola A, Pühringer J, Steiger M (2007) Gypsum: a review of its role in the  
534 deterioration of building materials. *Environ Geol* 52:339–352
- 535 Comodi P, Kurnosov A, Nazzareni S, Dubrovinsky L (2012) The dehydration process  
536 of gypsum under high pressure. *Phys Chem Miner* 39:65-71
- 537 Crupi V, Allodi V, Bottari C, D’Amico F, Galli G, Gessini A, La Russa M.F, Longo F,  
538 Majolino D, Mariotto G, Masciovecchio C, Pezzino A, Rossi B, Ruffolo S.A, Venuti V  
539 (2016) Spectroscopic investigation of Roman decorated plasters by combining FT-IR,  
540 micro-Raman and UV-Raman analyses. *Vib Spectrosc* 83:78-84
- 541 Doehne E, Price CA (2011) *Stone Conservation: An Overview of Current Research*,  
542 Second edition. Getty Conservation Institute.
- 543 Downs RT, Hall-Wallace M (2002) 18th General Meeting of the International  
544 Mineralogical Association, Edinburgh, Scotland. Programme With Abstracts, 128
- 545 EPA 2016 <https://www.epa.gov/pm-pollution> [last accessed July 2016]
- 546 Espinosa-Marzal R.M, Scherer G.W (2010) Advances in Understanding Damage by  
547 Salt Crystallization. *Acc Chem Res* 43:897-905
- 548 Flatt R.J (2002) Salt damage in porous materials: how high supersaturations are  
549 generated. *J Cryst Growth* 242:435-454 Franzén, LG (1990) Transport, deposition and  
550 distribution of marine aerosols over southern Sweden during dry westerly storms.  
551 *Ambio* 180–188
- 552 Gautam P, Blaha U, Appel E (2005) Magnetic susceptibility of dust-loaded leaves as a  
553 proxy of traffic-related heavy metal pollution in Kathmandu city, Nepal. *Atmos Environ*  
554 39:2201–2211
- 555 Gómez-Nubla L, Aramendia J, Fdez-Ortiz de Vallejuelo S, Castro K, Madariaga J.M  
556 (2013) From Portable to SCA Raman devices to characterize harmful compounds  
557 contained in used black slag produced in Electric Arc Furnace of steel industry. *J*  
558 *Raman Spectrosc* 44:1163-1171
- 559 ICOMOS, 2008. [http://www.icomos.org/en/component/content/article/116-english-](http://www.icomos.org/en/component/content/article/116-english-categories/resources/publications/261-monumentsasites-xv)  
560 [categories/resources/publications/261-monumentsasites-xv](http://www.icomos.org/en/component/content/article/116-english-categories/resources/publications/261-monumentsasites-xv). [last accessed July 2016]

1  
2  
3  
4  
5  
6  
7  
8  
9  
10  
11  
12  
13  
14  
15  
16  
17  
18  
19  
20  
21  
22  
23  
24  
25  
26  
27  
28  
29  
30  
31  
32  
33  
34  
35  
36  
37  
38  
39  
40  
41  
42  
43  
44  
45  
46  
47  
48  
49  
50  
51  
52  
53  
54  
55  
56  
57  
58  
59  
60  
61  
62  
63  
64  
65

561 Inza-Agirre A (2010) Estudio de series temporales y composición química del material  
562 particulado atmosférico en distintas áreas del País Vasco. Thesis, Universidad del País  
563 Vasco UPV/EHU

564 Larssen T, Lydersen E, Tang D, He Y, Gao J, Liu H, Duan L, Seip HM, Vogt RD,  
565 Mulder J, Shao M, Wang Y, Shang H, Zhang X, Solberg S, Aas W, Okland T, Eilertsen  
566 O, Angell V, Li Q, Zhao D, Xiang R, Xiao J, Luo J (2006) Acid Rain in China. Environ  
567 Sci Technol 40:418–425

568 Maguregui M, Sarmiento A, Martínez-Arkarazo I, Angulo M, Castro K, Arana G,  
569 Etxebarria N, Madariaga JM (2008) Analytical diagnosis methodology to evaluate  
570 nitrate impact on historical building materials. Anal Bioanal Chem 391:1361–1370

571 Maguregui M, Sarmiento A, Escribano R, Martinez-Arkarazo I, Castro K, Madariaga  
572 JM (2009) Raman spectroscopy after accelerated ageing tests to assess the origin of  
573 some decayed products found in real historical bricks affected by urban polluted  
574 atmospheres. Anal Bioanal Chem 395:2119–2129

575 Maguregui M, Prieto-Taboada N, Trebolazabala J, Goienaga N, Arrieta N, Aramendia J,  
576 Gomez-Nubla L, Sarmiento A, Olivares M, Carrero JA, Martinez-Arkarazo I, Castro K,  
577 Arana G, Olazabal MA, Fernandez LA, Madariaga JM (2010a) CHEMCH 1st  
578 international congress chemistry for cultural heritage, Ravenna

579 Maguregui M, Knuutinen U, Castro K, Madariaga JM (2010b) Raman spectroscopy as a  
580 tool to diagnose the impact and conservation state of Pompeian second and fourth style  
581 wall paintings exposed to diverse environments (House of Marcus Lucretius). J Raman  
582 Spectrosc 41:1400–1409

583 Maguregui M, Knuutinen U, Martínez-Arkarazo I, Castro K, Madariaga JM (2011)  
584 Thermodynamic and Spectroscopic Speciation to Explain the Blackening Process of  
585 Hematite Formed by Atmospheric SO<sub>2</sub> Impact: The Case of Marcus Lucretius House  
586 (Pompeii). Anal Chem 83:3319–3326

587 McAlister JJ, Smith BJ, Török A (2008) Transition metals and water-soluble ions in  
588 deposits on a building and their potential catalysis of stone decay. Atmos Environ  
589 42:7657–7668

1  
2  
3  
4  
5  
6  
7  
8  
9  
10  
11  
12  
13  
14  
15  
16  
17  
18  
19  
20  
21  
22  
23  
24  
25  
26  
27  
28  
29  
30  
31  
32  
33  
34  
35  
36  
37  
38  
39  
40  
41  
42  
43  
44  
45  
46  
47  
48  
49  
50  
51  
52  
53  
54  
55  
56  
57  
58  
59  
60  
61  
62  
63  
64  
65

590 Morillas H, Maguregui M, García-Florentino C, Carrero JA, Madariaga JM (2016a) The  
591 cauliflower-like black crusts on sandstones: A natural passive sampler to evaluate the  
592 surrounding environmental pollution. *Environ Res* 17:218-232

593 Morillas H, García-Galán J, Maguregui M, García-Florentino C, Marcaida I, Madariaga  
594 J.M (2016b) In-situ multianalytical methodology to evaluate the conservation state of  
595 the entrance arch of La Galea Fortress (Getxo, north of Spain). *Microchem J* 128:288-  
596 296

597 Morillas H, García-Galán J, Maguregui M, Marcaida I, García-Florentino C, Carrero  
598 J.A, Madariaga J.M (2016c) Evaluation of marine and urban-industrial environments  
599 influence on the conservation state of sandstone in Cultural Heritage Monuments using  
600 Handheld Energy Dispersive X-ray Fluorescence and other laboratory techniques.  
601 *Spectroschim Acta B* 123:76-88

602 Morillas H, Marcaida I, Maguregui M, Carrero JA, Madariaga JM (2016d) The  
603 influence of rainwater composition on the conservation state of cementitious  
604 building materials. *Sci Total Environ* 542:716-727

605 Morillas H, Maguregui M, García-Florentino C, Marcaida I, Madariaga JM (2016e)  
606 Study of particulate matter from Primary/Secondary Marine Aerosol and  
607 anthropogenic sources collected by a self-made passive sampler for the evaluation  
608 of the dry deposition impact on built heritage. *Sci Total Environ* 550:285-296

609  
610 Moropoulou A, Bisbikou K, Torfs K, Van Grieken R, Zezza F, Macri F (1998) Origin  
611 and growth of weathering crusts on ancient marbles in industrial atmosphere. *Atmos*  
612 *Environ* 32:967–982

613 Potgieter-Vermaak SS, Godoi RHM, Grieken RV, Potgieter JH, Oujja M, Castillejo M  
614 (2005) Micro-structural characterization of black crust and laser cleaning of building  
615 stones by micro-Raman and SEM techniques. *Spectrochim. Acta A* 61:2460–2467

616 Prieto-Taboada N, Gómez-Laserna O, Martínez-Arkarazo I, Olazabal MA, Madariaga  
617 JM (2014) Raman spectra of the Different Phases in the CaSO<sub>4</sub>-H<sub>2</sub>O system. *Anal*  
618 *Chem* 86:10131-10137

- 1  
2  
3  
4  
5  
6  
7  
8  
9  
10  
11  
12  
13  
14  
15  
16  
17  
18  
19  
20  
21  
22  
23  
24  
25  
26  
27  
28  
29  
30  
31  
32  
33  
34  
35  
36  
37  
38  
39  
40  
41  
42  
43  
44  
45  
46  
47  
48  
49  
50  
51  
52  
53  
54  
55  
56  
57  
58  
59  
60  
61  
62  
63  
64  
65
- 619 Querol X, Moreno T, Alastuey A, Gibbons W (2011) *Geoquímica Inorgánica*  
620 *Atmosférica: Elementos Trazadores de Fuentes Emisoras de Contaminantes*. *Macla*  
621 *14:143–144*
- 622 Rodríguez-Navarro C, Doehne E, Sebastian E (2000) How does sodium sulfate  
623 crystallize? Implications for the decay and testing of building materials. *Cement*  
624 *Concrete Res 30:1527-1534*
- 625 Ruffolo S.A, Comite V, La Russa M.F, Belfiore C.M, Barca D, Bonazza A, Crisci G.M,  
626 Pezzino A, Sabbioni C (2015) An analysis of the black crusts from the Seville  
627 Cathedral: A challenge to deepen the understanding of the relationships among  
628 microstructure, microchemical features and pollution sources. *Sci Tot Environ 502:157-*  
629 *166*
- 630 Saiz-Jimenez C, Garcia del Cura M.A (1991) Sulfated crusts: a microscopic, inorganic  
631 and organic analysis. In *Science, Technology and European Cultural Heritage*, ed. N.S.  
632 Baer, C. Sabbioni, A.I. Sors, Oxford, UK, Buitenworth-Heinemann 527-534
- 633 Sarmiento A, Maguregui M, Martinez–Arkarazo I, Angulo M, Castro K, Olazábal MA,  
634 Fernández LA, Rodríguez–Laso MD, Mujika AM, Gómez J, Madariaga JM (2008)  
635 Raman spectroscopy as a tool to diagnose the impacts of combustion and greenhouse  
636 acid gases on properties of Built Heritage. *J Raman Spectrosc 39:1042–1049*
- 637 Schiavon N, Chiavari G, Fabbri D (2004) Soiling of limestone in an urban environment  
638 characterized by heavy vehicular exhaust emissions. *Environ Geol 46:448–455*
- 639 Stefanis A, Theoulakis P, Pilinis C, (2005) The decay effects of sea-salt aerosol on the  
640 surface of historic buildings. *Proceedings of the 9th International Conference on*  
641 *Environmental Science and Technology Rhodes island, Greece A1391–A1396*
- 642 Sýkorová I, Havelcová M, Zeman A, Trejtnarová H (2011) Carbon air pollution  
643 reflected in deposits on chosen building materials of Prague Castle. *Sci Total Environ*  
644 *409:4606–4611*.
- 645 Watson JG, Chow JC, Chen LWA (2005) Summary of organic and elemental  
646 carbon/black carbon analysis methods and intercomparisons. *Aerosol Air Qual Res*  
647 *5:65–102*

648 Wein J, Wang A, Lambert JL, Wettergreen D, Cabrol NA, Warren-Rhodes K (2014)  
649 Mars Microbeam Raman Spectrometer (MMRS) on-board the Zöe Rover in the  
650 Atacama" in 11<sup>th</sup> International GeoRaman Conference, St. Louis, USA

651

652 **FIGURE CAPTIONS**

653

654 **Figure 1.** (a) Detail of the sampling location, (b) Malacate building and detail of its  
655 deteriorations patterns in sandstone, limestone and brick (from right to left), (c) Talaieta street  
656 building and a zoom of the soiling process and (d) Cemetery and detail of black crusts on it.

657 **Figure 1.** Raman spectra of samples of (A) Malacate's brick showing hematite, gypsum and  
658 (para)coquimbite or  $\gamma$ -anhydrite, (B) Malacates's sandstone showing carbon and gypsum, (C)  
659 Talaieta street's building showing hematite and (D) Talaieta street building showing anhydrite.

660 **Figure 2.** (A) SEM images of black crust on Malacate's sandstone showing a matrix of carbon  
661 layer. (B) Zoom of gypsum crystals on the pore. (C) Zoom of a deposited particle. (D) EDS  
662 spectrum depicting the main composition of Cl-particle in (C).

663 **Figure 4.** SEM image of the black crust on Malacate's limestone where the EDS punctual  
664 analyses were carried out, showing an aggregate of salts (A), gypsum (B) and calcite (c).

665 **Figure 5.** (A) SEM image of the cemetery gate's black crust showing random depositions. (B)  
666 Carbon EDS map highlighted in red (C) EDS spectra of selected particles on images A and (D)  
667 the pie chart of semi-quantitative information about the composition of aggregate particle 4  
668 obtained by EDS.

669 **Figure 6.** Soiling affected samples of Talaieta street building: (A) Ca EDS map (B) Si and S  
670 EDS maps overlapped on the same microscopic area as A (C) metallic particles identified by  
671 EDS on the same microscopic area (D) additional microscopic area focused with the SEM (E)  
672 EDS analysis of the particle circled in (D) (F) EDS spectrum of Fe particles from Figure C.

673 **Figure 7.** SEM images and the corresponding semi-quantitative composition (Atomic %)  
674 acquired by EDS analysis. Samples corresponding, to the soiling of the building of Talaieta  
675 street (1), black crust on the sandstone of the Malacate (2) and on the limestone of the cemetery  
676 gate (3).

677



